Rapid Recovery of Life at Ground Zero of the End Cretaceous Mass Extinction

Authors: Christopher, M. Lowery[1]*, Timothy J. Bralower[2], Jeremy D. Owens[3], Francisco J. Rodríguez-Tovar[4], Heather Jones[2], Jan Smit[5], Michael T. Whalen[6], Phillipe Claeys[7], Kenneth Farley[8,] Sean P. S. Gulick[1], Joanna V. Morgan[9], Sophie Green[10], E. Chenot[11], G. L. Christeson[1], C. S. Cockell[12], M. J. L. Coolen[13], L. Ferrière[14], C. Gebhardt[15], K. Goto[16], D. A. Kring[17], J. Lofi[18], R. Ocampo-Torres[19], L. Perez-Cruz[20], A. E. Pickersgill[21,22], M. H. Poelchau[23], A. S. P. Rae[9], C. Rasmussen[1], M. Rebolledo-Vieyra[24], U. Riller[25], H. Sato[26], S. M. Tikoo[27], N., Tomioka[28], J. Urrutia-Fucugauchi[20], J. Vellekoop[7], A. Wittmann[29], L. Xiao[30], K. E., Yamaguchi[31,32], W. Zylberman[33]

Affiliations:

[1]Institute for Geophysics, Jackson School of Geosciences, University of Texas at Austin, USA.
[2]Department of Geosciences, Pennsylvania State University, University Park, USA.
[3]Department of Earth, Ocean and Atmospheric Science | National High Magnetic Field Laboratory, Florida State University, Tallahassee, FL 32306, USA
[4]Departamento de Estratigrafía y Paleontología, Universidad de Granada, 18002 Granada, Spain
[5]Faculty of Earth and Life Sciences (FALW), Vrije Universiteit Amsterdam, Netherlands.
[6]Department of Geosciences, University of Alaska Fairbanks, USA.
[7]Analytical, Environmental and Geo-Chemistry, Vrije Universiteit Brussel, Brussels, Belgium.
[8]Division of Geological and Planetary Sciences, MS 170-25, California Institute of Technology Pasadena, CA 91125, USA
[9]Department of Earth Science and Engineering, Imperial College London, UK.
[10]British Geological Survey, Edinburgh, UK.
[11]Biogéosciences Laboratory, Université de Bourgogne-Franche Comté, Dijon, France.
[12]UK Centre for Astrobiology, School of Physics and Astronomy, University of Edinburgh, Edinburgh, UK.
[13]School of Earth and Planetary Sciences, WA-Organic and Isotope Geochemistry Centre (WA-OIGC), Curtin University, Bentley, Australia.
[14]Natural History Museum, Vienna, Austria.
[15]Alfred Wegener Institute Helmholtz Centre of Polar and Marine Research, Bremerhaven, Germany.
[16]International Research Institute of Disaster Science, Tohoku University, Sendai, Japan.
[17]Lunar and Planetary Institute, Houston, USA.
[18]Géosciences Montpellier, CNRS, Université de Montpellier, France.
[19]Groupe de Physico-Chimie de l´Atmosphère, L'Institut de Chimie et Procédés pour l'Énergie, l'Environnement et la Santé (ICPEES), Université de Strasbourg, France.
[20]Instituto de Geofísica, Universidad Nacional Autónoma De México, Ciudad de México, México.
[21] School of Geographical and Earth Sciences, University of Glasgow, UK.
[22]Argon Isotope Facility, Scottish Universities Environmental Research Centre (SUERC), East Kilbride, UK.
[23]Department of Geology, University of Freiburg, Germany.
[24]SM 312, Mza 7, Chipre 5, Resid. Isla Azul, Cancun, Quintana Roo, México, 77500

[25]Institut für Geologie, Universität Hamburg, Germany.
[26]Ocean Resources Research Center for Next Generation, Chiba Institute of Technology, Chiba, Japan
[27]Earth and Planetary Sciences, Rutgers University, New Brunswick, USA.
[28]Kochi Institute for Core Sample Research, Japan Agency for Marine-Earth Science and Technology, Kochi, Japan.
[29]LeRoy Eyring Center for Solid State Science, Physical Sciences, Arizona State University, Tempe, USA
[30] Planetary Science Institute, School of Earth Sciences, China University of Geosciences (Wuhan), China
[31]Department of Chemistry, Toho University, Chiba, Japan.
[32]NASA Astrobiology Institute, USA
[33]CNRS, Institut pour la Recherche et le Développement, Aix Marseille University, France.

*Correspondence to: cmlowery@utexas.edu

Abstract

The Cretaceous-Paleogene (K-Pg) mass extinction eradicated 76% of species on Earth[1,2]. It was caused by the impact of an asteroid[3,4] on the Yucatán carbonate platform in the southern Gulf of Mexico at 66.0 Ma[5] which formed the Chicxulub impact crater[6,7]. Following the mass extinction, recovery of the global marine ecosystem, measured in terms of primary productivity, was geographically heterogeneous[8], as export production in the Gulf of Mexico and North Atlantic/Tethys took 300 kyr to return to Late Cretaceous quantities, slower than most other regions[8-11]. Delayed recovery of marine productivity closer to the crater implies an impact-related environmental control, like toxic metal poisoning[12], on recovery times. Conversely, if no such geographic pattern exists, the best explanation for the observed heterogeneity is ecological, based on trophic interactions[13], species incumbency and competitive exclusion by opportunists[14], and "chance"[8,15,16]. Importantly, this question has bearing on the inherent predictability (or lack thereof) of future patterns of recovery in modern anthropogenically perturbed ecosystems. If there is a relationship between the distance from the impact and the recovery of marine productivity, we would expect recovery rates to be slowest in the crater itself. Here, we present

the first record of foraminifera, calcareous nannoplankton, trace fossils, and elemental abundance data from the first ~200 kyr of the Paleocene within the Chicxulub Crater. We show that life reappeared in the basin just years after the impact and a thriving, high-productivity ecosystem was established within 30 kyr, faster than many sites across the globe. This is a clear indication that proximity to the impact did not delay recovery and thus there was no impact-related environmental control on recovery. Ecological processes likely controlled the recovery of productivity after the K-Pg mass extinction and are therefore likely to be significant in the response of the ocean ecosystem to other rapid extinction events.

Main Text

The recent joint Expedition 364 of the International Ocean Discovery Program and International Continental Drilling Program recovered the first record of the few hundred thousand years immediately after the impact within the Chicxulub Crater. Site M0077, drilled into the crater's peak ring[7] (Extended Data Fig. 1), sampled a ~130 m thick generally upward-fining suevite (i.e., melt-bearing impact breccia) overlying impact melt rocks and fractured granite[17]. The boundary between the suevite and overlying earliest Paleocene pelagic limestone is in Core 40-1 (Fig. 1), and is comprised of a 76 cm upward-fining, brown, fine-grained, micritic limestone that we term the transitional unit. The lower portion of the transitional unit is laminated below 54 cm core depth and contains no trace fossils (Fig. 1, Extended Data Fig. 2). The laminations are thin graded beds with sub-mm scale cross bedding that indicate bottom currents and are likely due to the movement of wave energy, including tsunami and/or seiches, in the days after the impact. The fine grain size (primarily clay to silt, with some sand-sized grains concentrated in the graded beds) suggests that much of the material in the transitional unit was deposited from resuspension and settling. The transitional unit is overlain by a white pelagic

limestone. The lowermost sample taken in this limestone (34 cm) contains the planktic foraminifer *Parvularugolobigerina eugubina*, which marks the base of Zone Pα, as well as *P. extensa, P. alabamensis*, and *Guembelitria cretacea*. Because many other species that originate within Zone Pα first appear a few cm higher in the section (31-32 cm), we conclude that the base of the limestone lies very near the base of this zone, 30 kyr post-impact[18].

Biostratigraphy and basic assumptions about depositional and crater processes indicate that the transitional unit was deposited between several years and 30 kyr after impact (Fig. 2). To better constrain this, we utilize the abundance of extraterrestrial ^{3}He to determine sediment accumulation rates (see Methods). This proxy provides a firm upper limit of 8 kyr for deposition, assuming none of the ^{3}He is reworked. If even a small amount of ^{3}He is reworked (very likely, given the prevalence of reworked microfossils and impact debris), then the transitional unit was deposited in a period of time below the resolution of the method, < ~1 kyr. With no sediment source other than settling of material suspended by the impact and subsequent tsunami and seiches, a more realistic estimate for the duration of this unit is based on Stoke's law, which suggests ~6 years for the settling of a 2 μm grain of carbonate (an upper limit, as most grains are much larger; see SI for further discussion). The lower portion of the overlying limestone, which contains fossils which appear ~30 kyr post impact, appears conformable with the transitional unit and must therefore be condensed due to low pelagic sedimentation in the first few 10s of kyrs post impact.

Clear, discrete trace fossils, including *Planolites* and *Chondrites*, characterize the upper 20 cm of the transitional unit (above 54 cm) (Fig. 1, Extended Data Fig. 2), providing unequivocal evidence for benthic life in the crater within years of the impact. Flattening of the structures indicates that the traces were formed while the sediment was still soft, during or

shortly after deposition of the transitional unit. Infilling of the burrows with brown, fine-grained micrite also suggests traces were syndepositional and not derived from mixing of the Danian limestone above the transitional unit. Trace fossils produced during deposition of the limestone, as indicated by light infilling material, are distinct and only occur in the uppermost few cm of the transitional unit (Extended Data Fig. 2).

The transitional unit microfossils are dominated by clearly reworked Maastrichtian foraminifera and nannoplankton, known across the Gulf of Mexico and Caribbean as the K-Pg Boundary Cocktail[19] (Extended Data Fig. 3, Table S1). Although overall foraminiferal abundance (plotted as foraminifera per gram of sedimentary rock; Fig. 1) is high at the base of the unit, species known to range across the boundary ("survivor species") are rare in the lower transitional unit and become more common upsection even as total foraminifera decline (Fig. 1). Survivors, here defined as *Guembelitria cretacea*, *Muricohedbergella monmouthensis*, and *M. holmdelensis*[20], dominate a depauperate assemblage in the upper 20 cm of the transitional unit, coinciding with the first appearance of trace fossils (Extended Data Figs. 4 and 5).

The nannofossil assemblage in the transitional unit contains reworked Cretaceous specimens, including a group of clearly overgrown species that became extinct near the Campanian-Maastrichtian boundary, such as *Aspidolithus parcus* and *Eiffellithus eximius*. The remainder of the Cretaceous species, which dominate the assemblage, range to the top of or beyond the latest Maastrichtian (Table S2). Unusually small (<2 μm) and delicate specimens of *Micula* are observed throughout the transitional unit and increase in abundance upsection (Fig. 1), along with small *Retecapsa* (Extended Data Fig. 6). Taxa common at other sites in the earliest Danian are also present, including disaster genera like *Thoracosphaera* and *Braarudosphaera*.

Unlike the foraminifera, there are no clear stratigraphic trends in overall nannoplankton abundance (Fig. 1).

Because survivor species lived both before and after the K-Pg mass extinction, it is impossible to determine for certain if individual specimens in the transitional unit colonized the crater post-impact. However, the populations of foraminifera and nannoplankton are significantly different from those of the latest Cretaceous[12] (i.e., the expected population if the whole assemblage was reworked), suggesting that these taxa were true survivors (Fig. 1, Extended Data Fig. 6). *Guembelitria cretacea,* a common component of the survivor assemblage in the upper transitional unit, was restricted to marginal marine waters during the Maastrichtian and would not have been present at the pre-impact site, which was >100 m deep[21] and >500 km from shore[22]. The nannofossil assemblage in the transitional unit is significantly different from typical latest Maastrichtian assemblages, with some genera over-represented (*Watznaueria* and *Retecapsa*) and others under-represented (*Eiffellithus*, not including *E. eximius*, *Arkhangelskiella, Chiastozygus*, and *Prediscosphaera*) (Extended Data Fig. 6). Additionally, *Micula*, a robust taxon often used as a proxy for dissolution, is not as abundant as elsewhere, indicating that these unusual abundances are not due to poor or selective preservation (Extended Data Fig. 6).

This initial appearance of life is remarkably fast, especially because crater-specific factors do not seem to have had a negative impact on the local recovery of life. A vigorous, high-temperature hydrothermal system was established within the crater and may have persisted for millions of years after the impact[23], especially across the peak ring where rocks exhumed from deep in the crust were extensively fractured[7]. Nevertheless, the appearance of burrowing organisms within years of the impact indicates that the hydrothermal system did not adversely

affect seafloor life. Impact-generated hydrothermal systems are hypothesized to be potential habitats for early life on Earth[24] and on other planets, particularly below the surface. However, for marine impact craters in open ocean communication, like Chicxulub (Extended Data Fig. 1), our data indicate that locally significant but still comparatively small volumes of hydrothermal fluids were overwhelmed by the $1.3x10^4$ km^3 of well-mixed ocean water that filled the basin.

Likewise, the open connection with the Gulf of Mexico prevented the development of anoxia in the crater. Our analyses of iodine to calcium ratios suggest that local dissolved oxygen was high and stable in Zone Pα (Fig. 3). This is in contrast to the smaller (85-km wide) Eocene Chesapeake Bay impact crater in Virginia, USA, where anoxia due to restriction is attributed as the cause of delayed recovery of the benthic ecosystem on the crater floor[25]. This comparison suggests that the establishment of life within marine impact craters is controlled more by circulation (and thus crater geometry) than by the magnitude of the impact or global environmental effects.

The overlying pelagic limestone, which was deposited within Zone Pα (30-200 kyr post impact) contains abundant evidence of high productivity in a thriving ecosystem. The planktic foraminifer assemblage in Zone Pα is diverse and abundant (Fig. 3). Good preservation in the lowermost sample (34 cm) allowed the identification of over 60 species of benthic foraminifera, and benthics make up 12% of the assemblage at this level (Table S1). This percentage of benthics[26] and the overall benthic assemblage[27] are both typical of an upper to middle bathyal paleo water depth (~600-700 m)[10,27]. At this level, trace fossils increase in size, abundance, and diversity. The abundance and diversity of benthic organisms indicate that by ~30 kyr after the impact, seafloor conditions had returned to normal and sufficient organic matter flux existed to sustain a diverse, multilayer benthic community.

Conversely, the nannoplankton assemblage in the Danian limestone is dominated by *Braarudosphaera* and calcareous dinoflagellate cysts (e.g., *Thoracosphaera*), common disaster taxa in the early recovery interval. Large, foraminifer-sized calcispheres appear after ~100 kyr. Calcareous phytoplankton in the earliest Danian clearly represent a low-diversity, high-productivity bloom. Genera like *Neobiscutum* and *Prinsius*, common bloom taxa in the recovery interval at other Northern Hemisphere sites, do not become common until several meters higher in the section, >1 myr after the impact. Organic microfossils are completely absent from the study interval, likely due to poor preservation of organic material.

Geochemical paleoproductivity proxies, particularly Ba/Ti and Ba/Fe ratios, also indicate high productivity in the post-impact Danian limestone (Fig. 1). Ba/Ti ratios of ~1.0 at the base of the limestone (~30 kyr post impact) and ~2.0 above that (15 cm higher or ~100 kyr post impact) indicate relatively high and increasing productivity in the Chicxulub Basin in the earliest Danian.

The recovery of productivity in the crater is faster than at many sites, including those in the Gulf of Mexico, some of which took 300 kyr or more to recover to a similar extent[8,11]. Therefore, we find that proximity to the impact was not a control on recovery in marine ecosystems. The wide range of rates of recovery in the oceans show no relationship with geographic distance to the crater and so are best explained by natural ecological interactions between organisms within recovery ecosystems like incumbency and competitive exclusion[8,14]. These trends can be used to understand the rates of recovery after other major extinction events and, critically, predict the long-term recovery of modern ecosystems affected by pollution and climate change.

Methods

IODP-ICDP Expedition 364 drilled the peak ring of the Chicxulub crater in the spring of 2016 (Extended Data Fig. 1). Samples were taken at the Bremen IODP Core Repository during the Exp. 364 sampling party. Core depth in centimeters, with zero at the top of the section (616.24 m below sea floor), are reported throughout. Core material was indurated, and ~0.5 cm quarter-rounds were cut out with a rock saw. Due to the need to reserve core material for rare earth element geochemistry (which will be presented in a separate manuscript), the lowermost ~1.5 cm of the Danian limestone was not sampled. Individual samples were subdivided for foraminifer, calcareous nannoplankton, and discrete geochemical analyses.

Forty-three samples were examined for planktic and benthic foraminifera from Core 40 from 0-110 cm depth. Samples were weighed, crushed with a mortar and pestle, soaked overnight (or longer) in a 10% solution of hydrogen peroxide buffered with borax, and washed over a 43 μm sieve to ensure capture of small Danian taxa. The sieve was soaked in methylene blue dye between samples to identify contaminated specimens. Samples were then dried in an oven, split to obtain a manageable volume of material, and examined for foraminifera, calcispheres, and other sand-sized particles. In the Danian limestone, at least 300 specimens were counted to establish a statistically robust population[28] and the rest of the residue was then examined for biostratigraphically significant taxa. Low abundances in the transitional unit precluded 300 specimen counts. However, we demonstrate that our values are sufficient to reject the null hypothesis (that the observed enrichments in survivor taxa are the result of random noise) with binomial confidence limits. This calculation traditionally provides the basis for the 300-specimen "rule:" counting 300 specimens provides statistical confidence at a 95% confidence interval that a species that makes up 1% of the population is represented in the count[28]. As we show, fewer specimens are sufficient to demonstrate the presence of a survivor

population in our samples. Binomial confidence limits for samples with fewer than 300 specimens are reported in Table S1. Additionally, a single unusually well-preserved sample at the base of the post-impact limestone was examined for rare benthic species to determine the true diversity of benthics at the base of the unit (Table S1). Planktic foraminifer biozonation follows the P Zones of Berggren and Pearson[29] as modified by Wade et al.[18].

Ninety-seven samples were examined for nannofossils. Samples were disaggregated in water and smear slides were made from the supernatant. Slides were observed in a transmitted light microscope at 1600x until at least 100 specimens were observed (Table S2). Standard taxonomy was applied (http://www.mikrotax.org/Nannotax3/index.php?dir=Coccolithophores). The abundance of taxa at Site M0077 was compared to the global K-Pg nannoplankton compilation of Jiang et al.[12].

Ichnological analysis was conducted from 0-110 cm. Ichnological observations were conducted on core material and a detailed and continuous analysis of digital images. To improve visibility of ichnological features, images were treated by a digital image methodology, based on modification of image adjustments as levels, brightness and vibrance[30,31]. Ichnotaxonomical classification of trace fossils was based on the overall shape and the presence of diagnostic criteria such as size and presence of branches[32]. Special attention was given to the infilling material of biogenic structures.

The measurement of I/(Ca+Mg) was carried out using a procedure similar to that described by Lu et al.[33]. For each sample and geostandard approximately 3-4 mg of carbonate powder was weighed out, dissolved in ~0.45M nitric solution, and then diluted using 0.1M nitric acid and 0.5% TMAH solution. All reported measurements are with samples that had a matrix of 50 ± 5 ppm Ca solution to ensure the most precise iodine measurement. Dissolved samples had

TMAH solution added within an hour to avoid any possible loss of volatilized iodine[33]. Samples were measured using an Agilent inductively coupled plasma mass spectrometer 7500cs housed within the geochemistry group of the National High Magnetic Field Laboratory at Florida State University. A previously reported known sample, Key Largo (KL 1-1) was used to ensure reliable reproducibility. Our value of 5.51 μmol/mol was within error of the reported value of 5.55 μmol/mol (*46*). Hardisty et al.[34] found that a generally low oxygen conditions correspond to ~2.6 μmol/mol for I/(Ca+Mg). Values are reported in Table S3.

Section 1 of Core 40 was scanned with an AVAATECH XRF Core Scanner II at MARUM, Bremen, Germany during the onshore phase of Expedition 364 (Fig. 1). The split core was covered with a 4 μm thick SPEX CertiPrep Ultralene foil to avoid contamination. XRF data was acquired with a Canberra X-PIPS silicon drift detector with 1550 eV resolution, a Canberra DAS 1000 digital spectrum analyzer, and an Oxford Instruments 50W XTF011 X-ray tube with rhodium target material. X-ray spectra were processed with WIN AXIL software from Canberra Erisys at a resolution of 12 mm and a step of 10 mm. Scans were conducted at different voltages to determine a range of element concentrations: 50 kV, with a beam current of 1 mA (Ba and Sr; average dead time of 5%), and 10 kV with a beam current of 0.15 mA (Al, Si, K, Ca, Ti, Fe, Mn, and S; average dead time of 11%). For each scan, sampling time was 20 seconds per spot.

^{3}He is delivered to the Earth's surface by cosmic dust grains and over short time spans (~ Myr) can be used as a constant flux proxy[35]. Previous work has shown that the K-Pg impactor was not associated with enhanced ^{3}He flux, and the mean extraterrestrial ^{3}He flux from cosmic dust accretion at the end of the Cretaceous (106 x10^{-15} cc STP/g/cm^{2}/kyr) was used to estimate the duration over which the K-Pg boundary clay was deposited at Gubbio and El Kef[36]. We use a

similar approach here to establish the sedimentation rate of the transitional unit, which we use to develop an age model.

Helium isotope ratios and concentrations were measured on ~1g aliquots of sediment following standard analytical procedures[31]. Extraterrestrial ^{3}He concentrations were computed from measured He isotopic compositions using an isotopic deconvolution model[36]. Results are shown in Extended Data Table 1. ^{3}He concentrations and ^{3}He/^{4}He ratios are generally low compared to typical marine sediments of similar age[37,38]. Nevertheless, with the exception of the lowest sample in the transitional unit (106.5 cm), the fraction of ^{3}He attributable to an extraterrestrial source is high, ranging from ~0.70 to 0.96. The deepest sample has a similar ^{3}He concentration to other samples in the transitional unit, but ~5 times more ^{4}He. This elevated ^{4}He likely arises from a higher concentration of terrigenous ^{4}He-bearing material deposited rapidly after the impact.

We see no evidence for extraterrestrial He carried in impactor fragments, such as highly elevated and/or highly variable ^{3}He and ^{3}He/^{4}He ratios. The absence of such a signal is consistent with either a) the absence of impactor fragments in the material analyzed, or b) loss of extraterrestrial ^{3}He from the impactor via heating, vaporization or fusion. Note that, unlike many tracers of the impactor (such as Ir), deposition of fused or vaporized impactor will leave no trace in the sedimentary record because once He is lost into the atmosphere, it can no longer be retained in sediments.

References and Notes:

1. Jablonski, D. Extinctions in the fossil record *in* Lawton, J. H. & May, R. M. Eds., *Extinction Rates*, New York, Oxford University Press, 25-44 (1995).

2. Schulte, P. et al. The Chicxulub asteroid impact and mass extinction at the Cretaceous-Paleogene Boundary, *Science* **327**, 1214-1218 (2010).

3. Alvarez, L. W., Alvarez, W., Asaro, F. & Michel, H. V. Extraterrestrial cause for the Cretaceous/Tertiary extinction, *Science* **208**, 1095-1108 (1980).

4. Smit, J. & Hertogen, J. An extraterrestrial event at the Cretaceous-Tertiary boundary, *Nature* **285**, 198-200 (1980).

5. Renne, P. R. et al. Time scales of critical events around the Cretaceous-Paleogene Boundary, *Science,* **339**, 684-687 (2013).

6. Hildebrand, A. R. et al. Chicxulub Crater: A possible Cretaceous/Tertiary boundary impact crater in the Yucatán Peninsula, Mexico, *Geology* **19**, 867-871 (1991).

7. J. Morgan, et al. The formation of peak rings in large impact craters, *Science* **354**, 878-882 (2016).

8. Hull, P. M. & Norris, R.D. Diverse patterns of ocean export productivity change across the Cretaceous-Paleogene boundary: New insights from biogenic barium, *Paleoceanography* **26** PA3205 (2011).

9. Alegret, L. & Thomas, E. Cretaceous/Paleogene boundary bathyal paleo-environments in the central North Pacific (DSDP Site 465), the northwestern Atlantic (ODP Site 1049), the Gulf of Mexico, and the Tethys: The benthic foraminiferal record, *Palaeogeography, Palaeoclimatology, Palaeoecology* **224**, 53-82 (2005).

10. Alegret, L. Molina, E. & Thomas, E. Benthic foraminifera at the Cretaceous-Tertiary boundary around the Gulf of Mexico, *Geology*, **29**, 891-894 (2001).

11. Alegret, L. Arenillas, I. Arz, J.A. & Molina, E. Foraminiferal event-stratigraphy across the Cretaceous/Paleogene boundary, *Neues Jahrbuch für Geologie und Paläontologie – Abhandlungen* **231**, 25-50 (2004).

12. Jiang, S. Bralower, T. J. Patzkowsky, M. E., Kump, L. R. & Schueth, J.D. Geographic controls on nannoplankton extinction across the Cretaceous/Paleogene Boundary, *Nature Geoscience* **2010**, 280-285 (2010).

13. Solé, R. V. Montoya, J. S. & Erwin, D. H. Recovery after mass extinction: evolutionary assembly in large-scale biosphere dynamics, *Philosophical Transactions of the Royal Society of London* **357**, 697-707 (2002).

14. Schueth, J. D. Bralower, T. J., Jiang, S. & Patzkowsky, M. E. The role of regional survivor incumbency in the evolutionary recovery of calcareous nannoplankton from the Cretaceous/Paleogene (K/Pg) mass extinction, *Paleobiology* **41**, 661-679 (2015).

15. Hull, P. M. Norris, R.D., Bralower, T. J. & Schueth, J.D. A role for chance in marine recovery from the end-Cretaceous extinction, *Nature Geoscience* **4**, 856-860 (2011).

16. Yedid, G., Ofria, C. A. & Lenski, R. E. Selective press extinctions, but not random pulse extinctions, cause delayed ecological recovery in communities of digital organisms, *The American Naturalist* **173**, E1 (2009).

17. Gulick, S. P. S. et al. *Expedition 364 Preliminary Report: Chicxulub: Drilling the K-Pg Impact Crater*, International Ocean Discovery Program, doi:10.14379/iodp.pr364.2017 (2017).

18. Wade, B. S., Pearson, P. N., Berggren, W. A. & Pälike, H. Review and revision of Cenozoic tropical planktonic foraminiferal biostratigraphy and calibration to the geomagnetic polarity and astronomical time scale, *Earth Science Reviews* **104**, 111-142 (2011).

19. Bralower, T. J., Paull, C. K. & Leckie R. M. The Cretaceous-Tertiary boundary cocktail: Chicxulub impact triggers margin collapse and extensive sediment gravity flows, *Geology*, **26**, 331-334 (1998).

20. Olsson, D. K., Hemleben, C., Berggren, W. A. & Huber, B. T. *Atlas of Paleocene Planktonic Foraminifera*, Smithsonian Contributions to Paleobiology **85**, (1999).

21. Gulick, S. P. S. et al. Importance of pre-impact crustral structure for the asymmetry of the Chicxulub impact crater, *Nature Geoscience*, **1**, 131-135 (2008).

22. Sohl, N. Upper Cretaceous, *Geology of North America, Volume J: Gulf of Mexico Basin* 205-244 (1991).

23. Abramov, O. & Kring, D. A., Numerical modeling of impact-induced hydrothermal activity at the Chicxulub crater, *Meteoric and Planetary Science* **42**, 93-112 (2007).

24. Cockell, C. S. The origin and emergence of life under impact bombardment, *Phil. Trans. R. Soc. B* **361**, 1845-1856 (2006).

25. Poag, C. W. Paleoenvironmental recovery from the Chesapeake Bay bolide impact: The benthic foraminiferal record, in Gohn, G. S., Koeberl, C., Miller, K. G. & Reimold, W. U. Eds., The ICDP-USGS Deep Drilling Project in the Chesapeake Bay Impact Structure: Results from the Eyreville Core Holes, *The Geological Society of America Special Paper* **458**, 747-773 (2009).

26. Leckie, R.M. & Olson, H. C. Foraminifera as proxies for sea level change on siliciclastic margins, *SEPM Special Publication* **75**, 5-19 (2003).

27. Alegret, L. & Thomas, E. Upper Cretaceous and lower Paleocene benthic foraminifera from northeastern Mexico, *Micropaleontology* **47**, 269-316 (2001).

Methods References

28. Buzas, M. A. Another look at confidence limits for species proportions, *Journal of Paleontology*, **64**, 842-843 (1990)

29. Berggren, W. A. & Pearson, P. N. A revised tropical and subtropical Paleogene planktonic foraminiferal zonation, *Journal of Foraminiferal Research* **35**, 279-298 (2005).

30. Dorador, J. & Rodríguez-Tovar, F. Digital image treatment applied to ichnological analysis of marine core sediments *Facies*, **60**, 39-44 (2014).

31. Dorador, J. & Rodríguez-Tovar, F. J. Stratigraphic variation in ichnofabrics at the "Shackleton Site" (IODP Site U1385) on the Iberian Margin: Paleoenvironmental implications, *Marine Geology* **377** 118-126 (2016).

32. Knaust, D. *Atlas of Trace Fossils in Well Core: Appearance, Taxonomy and Interpretation*, Springer (2017).

33. Lu, Z. Jenkyns, H. C. & Rickaby, R. E. M. Iodine to calcium ratios in marine carbonate as a paleo-redox proxy during oceanic anoxic events. *Geology* **38**, 1107–1110, doi:10.1130/g31145.1 (2010).

34. Hardisty, D. S. et al. Perspectives on Proterozoic surface ocean redox from iodine contents in ancient and recent carbonate. *Earth and Planetary Science Letters* **463**, 159-170, doi: 10.1016/j.epsl.2017.01.032 (2017).

35. Farley, K. A. & Eltgroth, S. F. An alternative age model for the Paleocene-Eocene thermal maximum using extraterrestrial ^{3}He, *Earth and Planetary Science Letters*, **208** 135-148 (2003).

36. Patterson, D. B. & Farley, K. A. Extraterrestrial ^{3}He in seafloor sediments: Evidence for correlated 100 kyr periodicity in the accretion rate of interplanetary dust, orbital parameters, and Quaternary climate, *Geochimica et Cosmochimica Acta*, **62**, 3669-3682 (1998).

37. Mukhopadhyay, S. Farley, K. A. & Montanari, A. a 35 Myr record of helium in pelagic limestones from Italy: Implications for interplanetary dust accretion from the early Maastrichtian to the middle Eocene, *Geochimica et Cosmochimica Acta*, **65** 653-669 (2001a).

38. Mukhopadhyay, S. Farley, K. A. & Montanari, A. A short duration of the Cretaceous-Tertiary boundary event: Evidence from extraterrestrial Helium-3, *Science* **291** 1952-1955 (2001b).

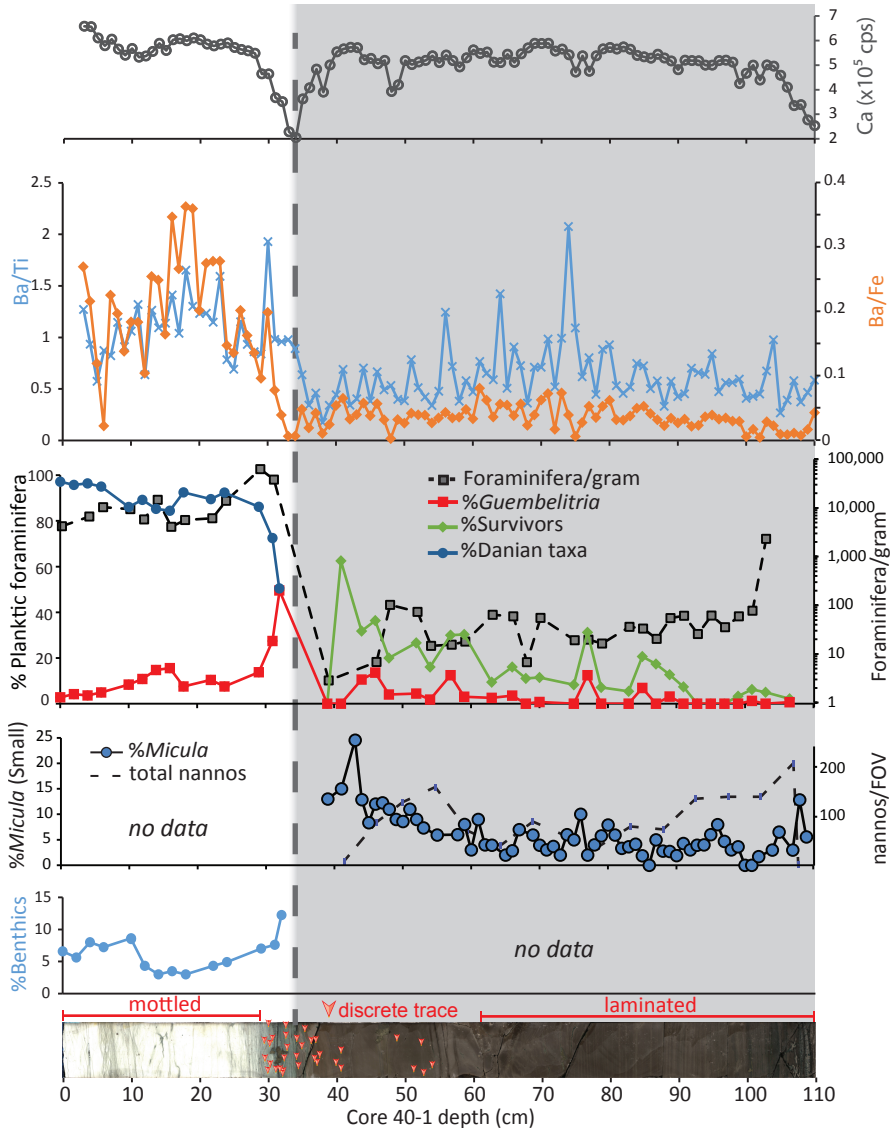

Fig. 1. **Paleoproductivity indicators in the earliest Paleocene at Site M0077**. The shaded area is the transitional unit and the dashed line represents the contact with the overlying pelagic limestone. Top to bottom: XRF-derived calcium abundance in counts per second (cps); Ba/Ti and Ba/Fe ratios; %abundances key planktic foraminiferal groups, including %*Guembelitria*, %survivors (i.e., Cretaceous species known to survive the impact), and % Danian taxa (i.e., species which evolved after the impact), as percentage of total foraminifera; foraminifera per gram of sediment, plotted on a log scale; %*Micula* smaller

than 2μm (against total nannoplankton) and nannoplankton abundance (total occurrences per field of view – FOV); %benthic foraminifera (against total foraminifera); Core image of 364-M0077A-40R-1 0-110 cm Core 40R-1, 34 to 110 cm (616.58 to 617.33 meters below seafloor) with discrete trace fossils highlighted by arrows (see Extended Data Fig. 2 for larger version of this image).

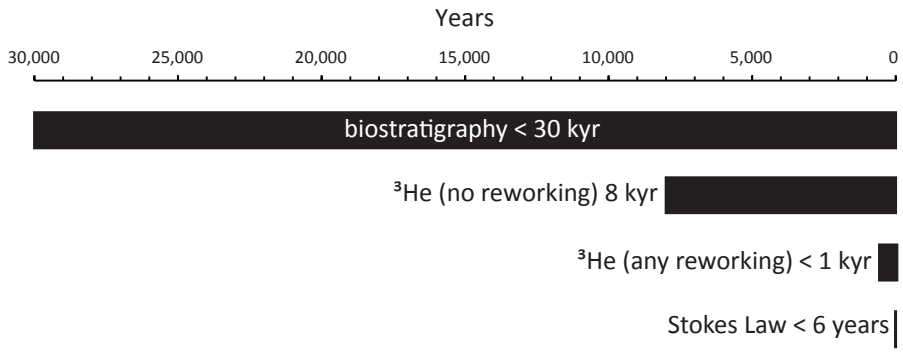

Figure 2. Constraints on the age of the transitional unit. Maximum durations of the transitional unit based on biostratigraphy (which suggests it was deposited in less than 30 kyr), extra-terrestrial 3He (which suggests it was deposited in approximately 8 kyr if there is no reworking, or less than 1 kyr if there is any reworking) and Stokes' law, which suggests it was deposited in less than 6 years.

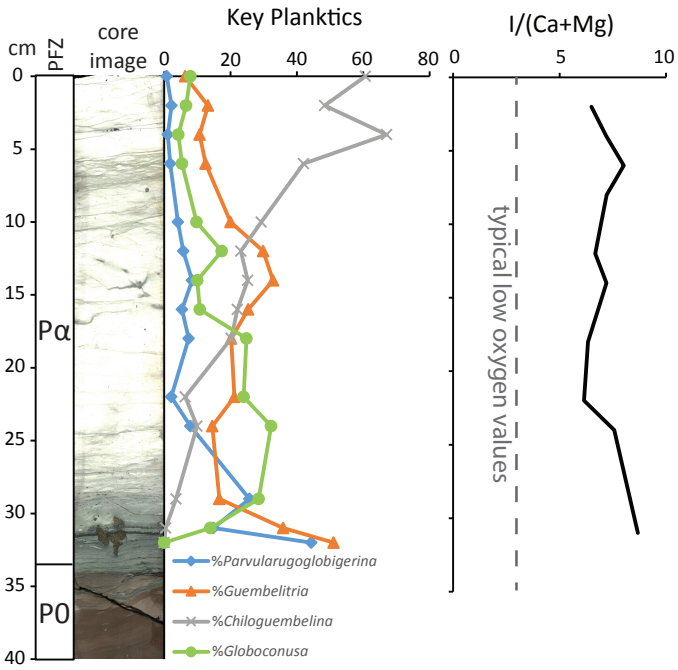

Figure 3. Early Danian foraminifer abundances and I/(Ca+Mg) oxygenation proxy. Left: Key Danian planktic foraminifera. Normal perforate planktics (*Eoglobigerina, Globanomalina, Parasubbotina,* and *Praemurica*) are rare throughout the study interval and not plotted here; all are plotted as % total planktic foraminifera. Right: I/(Ca+Mg) redox proxy, indicating well-oxygenated conditions in the Chicxulub crater through this interval. PFZ, planktic foraminfer zone.

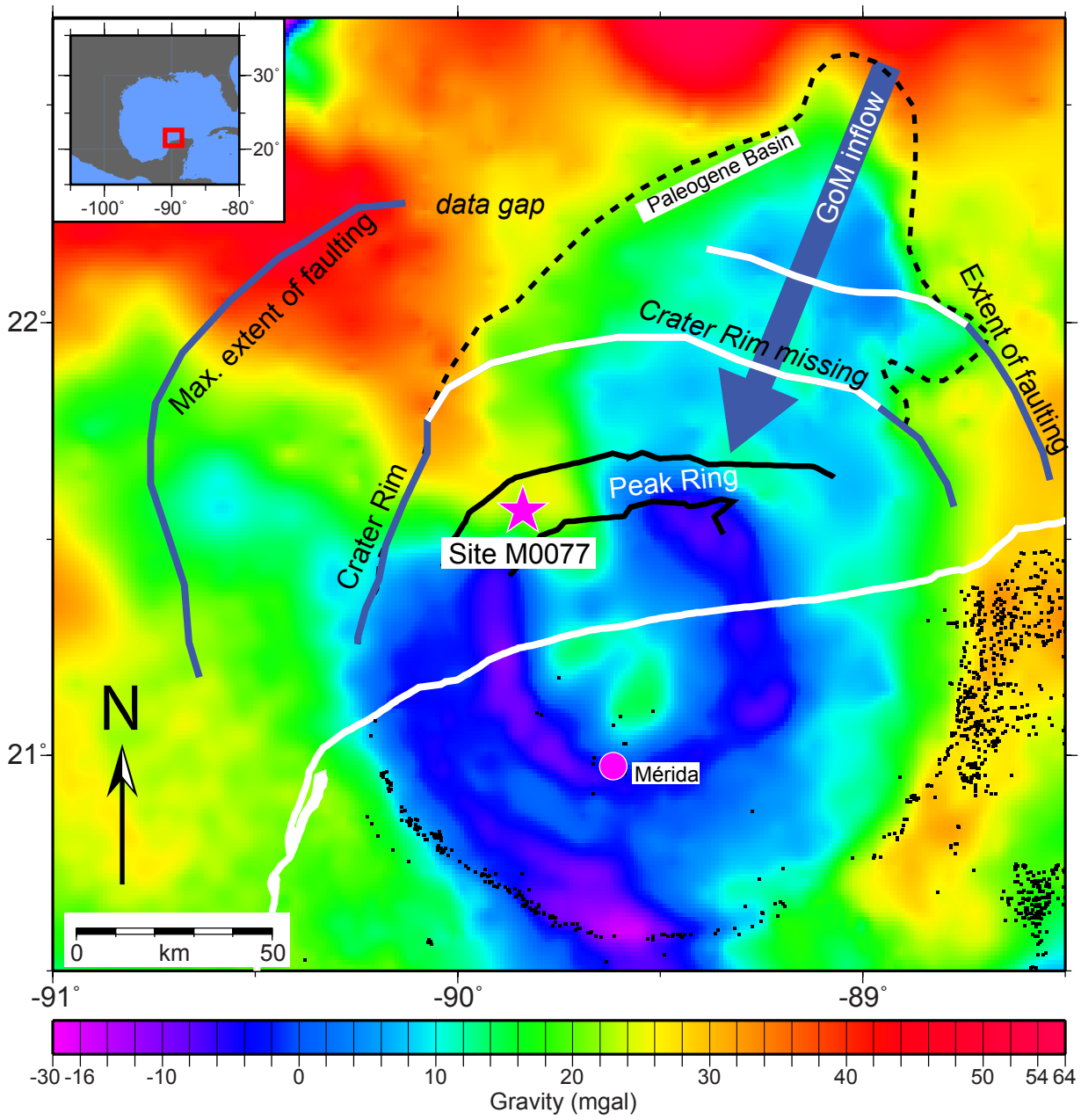

Extended Data Figure 1. Location of Site M0077 in the Chicxulub Crater as seen on gravity data. Black dots are cenotes. Modified from Gulick et al.[21].

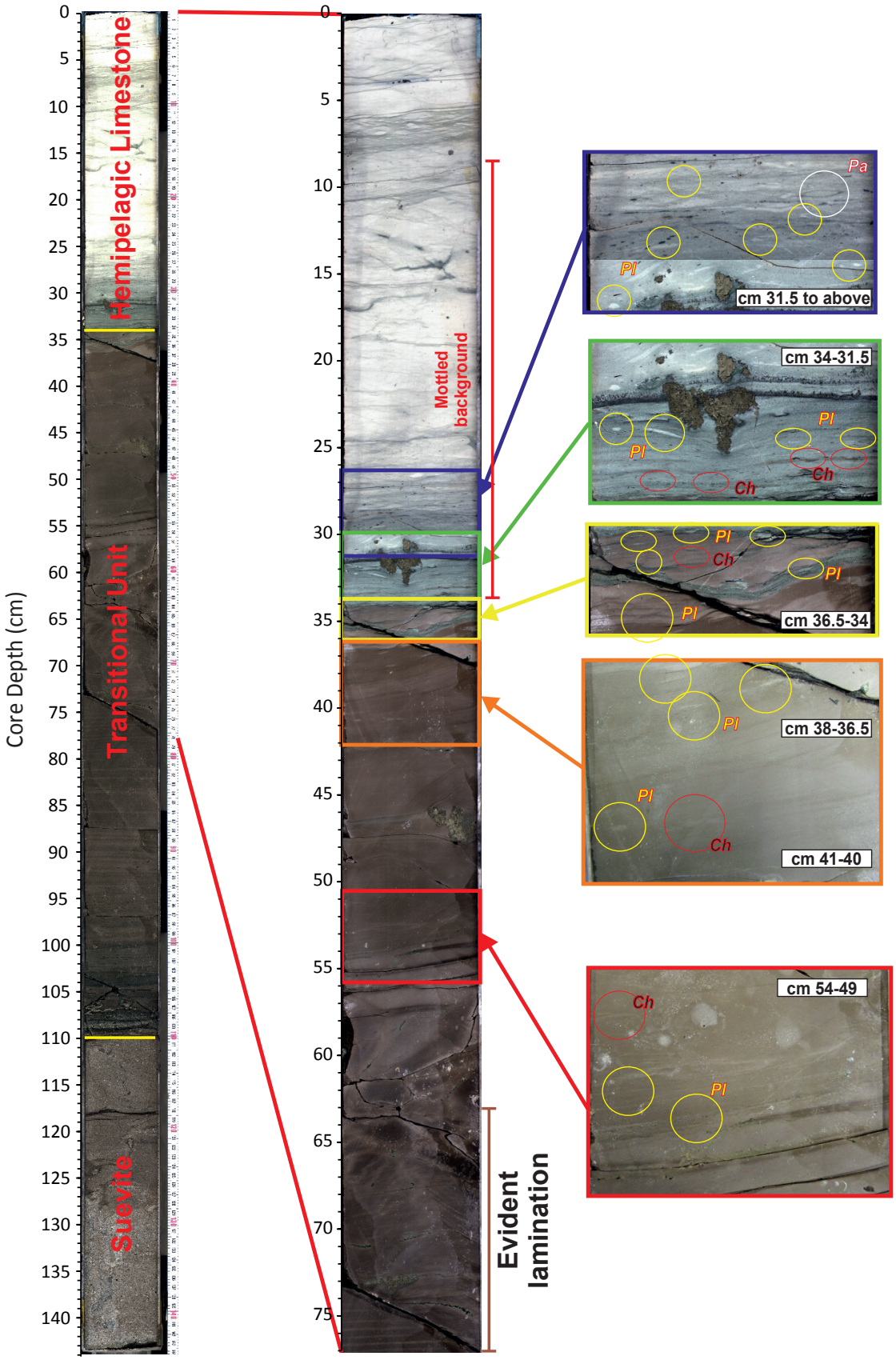
Core Depth (cm)
Hemipelagic Limestone
Transitional Unit
Sapropel
Mottled background
Evident lamination
Pa
Pl
cm 31.5 to above
cm 34-31.5
Ch
cm 36.5-34
cm 38-36.5
cm 41-40
cm 54-49

Extended Data Figure 2. Trace fossils in Core 40 Section 1 of IODP Hole M0077A. Discrete burrows in the upper transitional unit and the lower limestone are circled and labelled by the genus. Above the base of the limestone, trace fossils are abundant; representative examples are highlighted in the lower 10 cm of this interval. Ch*: Chondrites***;** Pl: *Planolites*; Pa: *Paleophycus*.

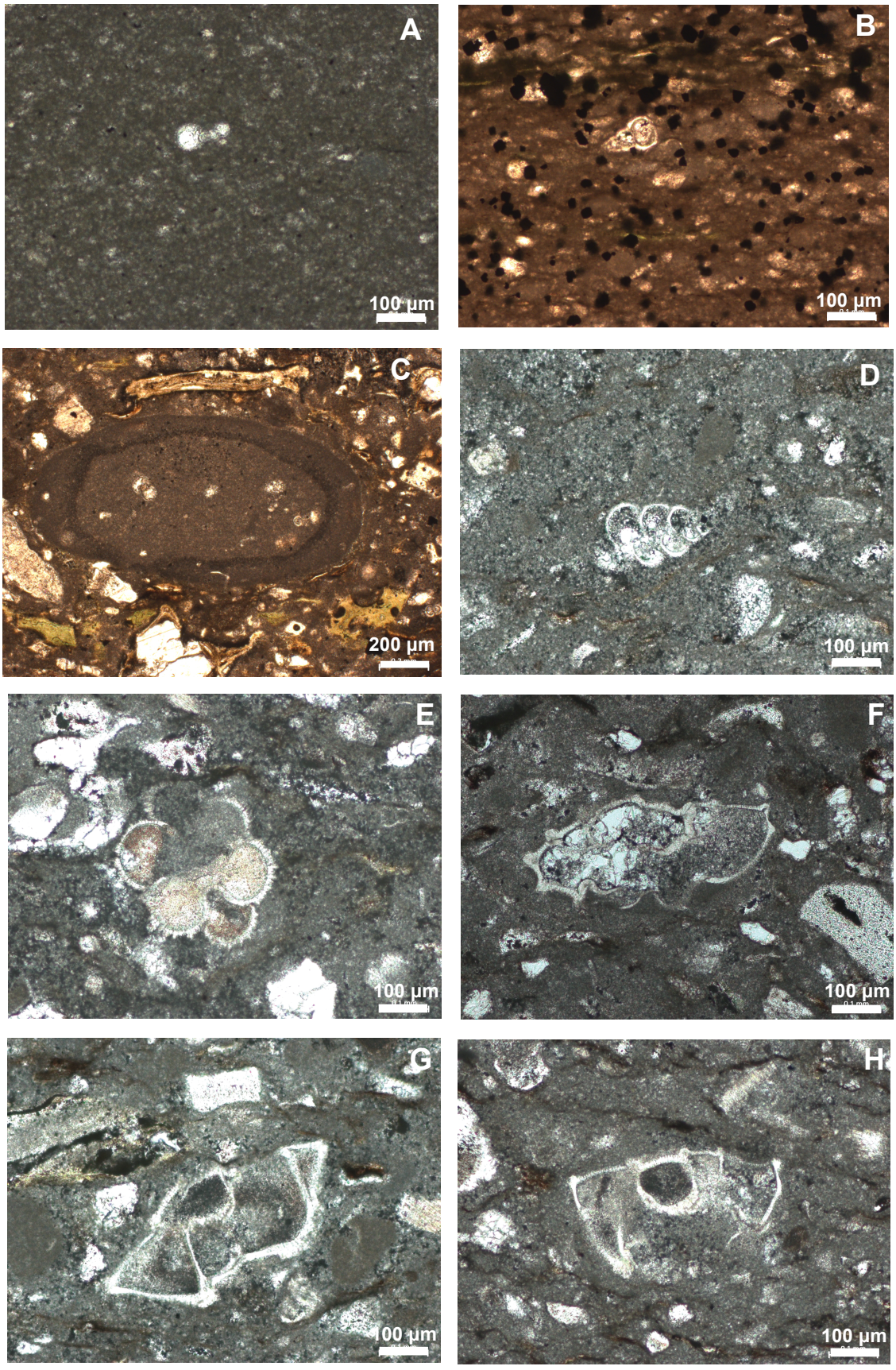
A
100 µm
B
100 µm
C
200 µm
D
100 µm
E
100 µm
F
100 µm
G
100 µm
H
100 µm

Extended Data Figure 3. Reworked Cretaceous foraminifera in the transitional unit. A *Globigerinelloides* sp., 364-M0077A-40R-1-W 55-56 cm; **B** *Heterohelix* sp. 364-M0077A-40R-1-W 104-105 cm; **C** clast of pelagic limestone containing older Cretaceous planktic foraminifera 364-M0077A-40R-1-W 106-110 cm; **D** *Praegublerina pseudotessera* 364-M0077A-40R-1-W 118-129cm ; **E** *Racemiguembelina powelli* 364-M0077A-40R-1-W 118-129 cm; **F** *Globotruncana bulloides* 364-M0077A-40R-1-W 110-118 cm; **G** *Globotruncanita stuartiformis* 364-M0077A-40R-1-W 118-129 cm; **H** *Globotruncanita elevata* 364-M0077A-40R-1-W 118-129 cm. Scale bars, 100 μm.

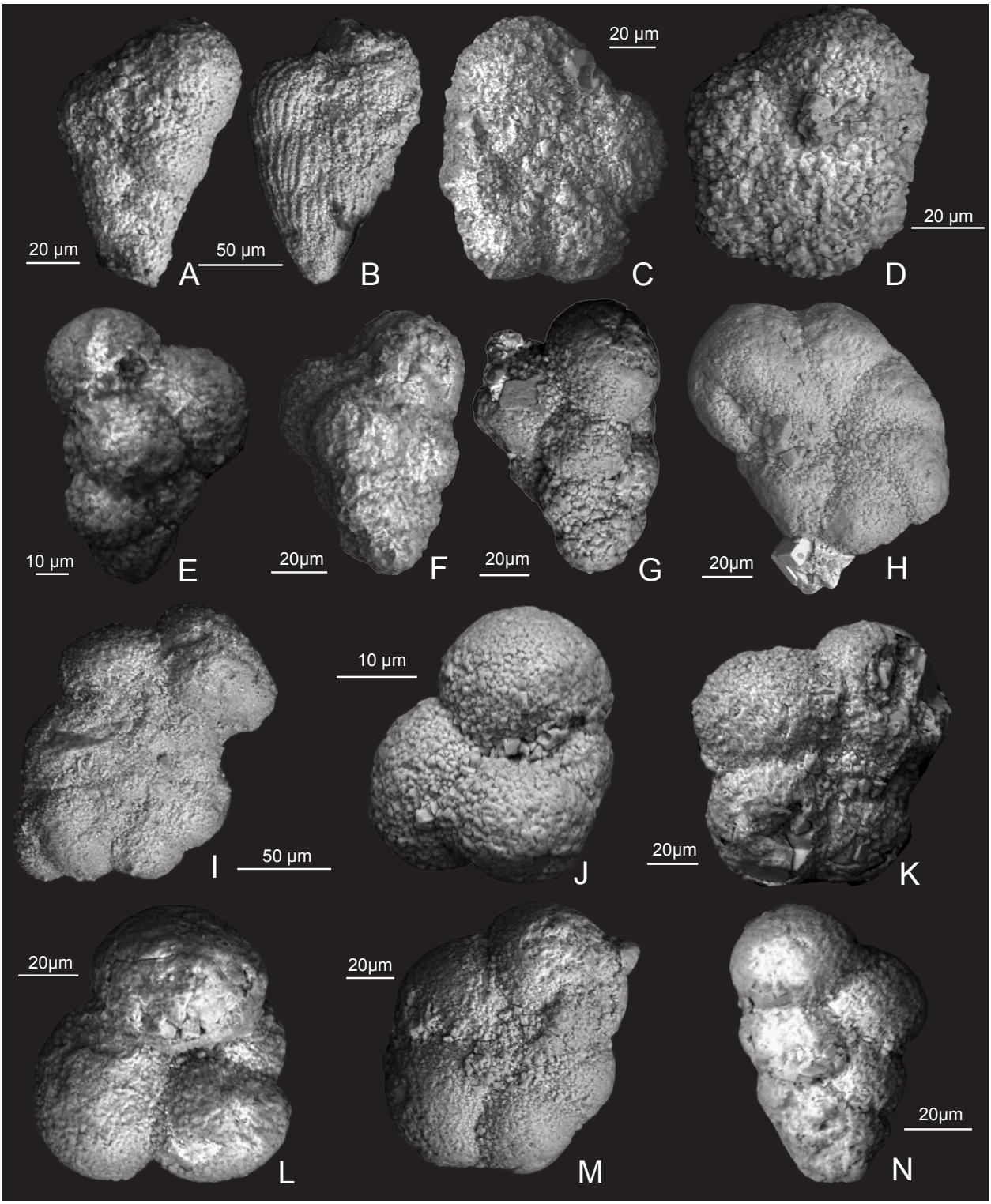

Extended Data Figure 4. Scanning electron micrographs of planktic foraminifera from Core 40. **A-B**, examples of common reworked Cretaceous biserials, 364-M0077A-40R-1

102-103 cm; **C** *Muricohedbergella monmouthensis* 364-M0077A-40R-1-W 102-103 cm; **D** *Muricohedbergella holmdelensis* 364-M0077A-40R-1-W 44-45 cm; **E** *Guembelitria cretacea* 364-M0077A-40R-1-W 44-45; **F** *Guembelitria cretacea* 364-M0077A-40R-1-W 29-30 cm; **G** *Guembelitria cretacea* 364-M0077A-40R-1-W 29-30 cm; **H** *Parvularugoglobigerina eugubina* 364-M0077A-40R-1-W 31-32 cm; **I** *Parvularugoglobigerina eugubina* 364-M0077A-40R-1-W 31-32 cm; **J** *Globoconusa daubjergensis* 364-M0077A-40R-1-W 31-32 cm; **K** *Eoglobigerina eobulloides* 364-M0077A-40R-1-W 29-30 cm; **L** *Eoglobigerina edita* 364-M0077A-40R-1-W 29-30 cm; **M** *Praemurica taurica* 364-M0077A-40R-1-W 10-11 cm; **N** *Chiloguembelina morsei* 364-M0077A-40R-1-W 10-11 cm.

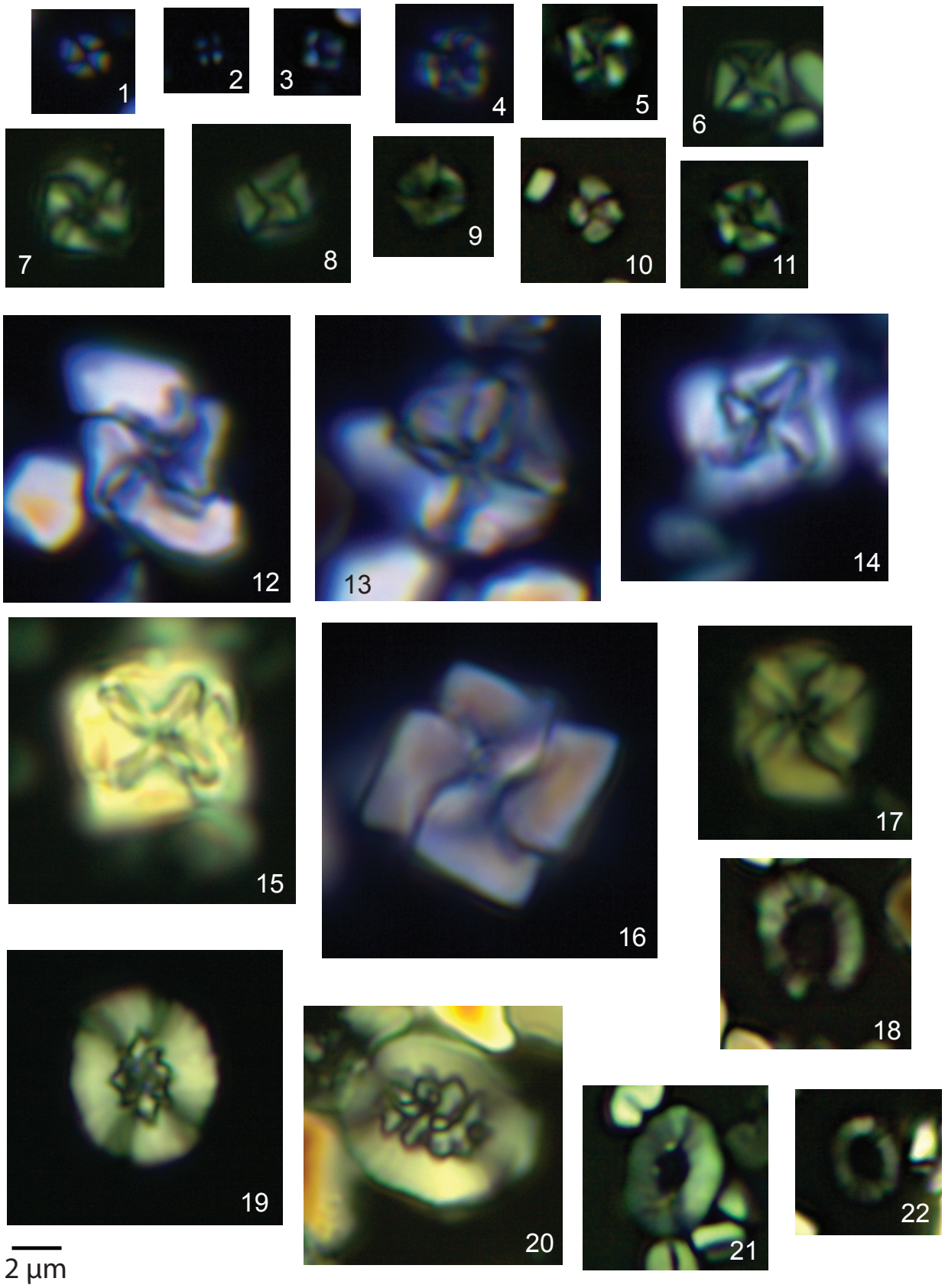
1
2
3
4
5
6
7
8
9
10
11
12
13
14
15
16
17
18
19
20
21
22
2 µm

Extended Data Figure 5. Small and regular sized nannofossils in the transitional unit. All photographs from Core 364-M0077-40R-1-W. Plates 1-11, small *Micula* spp. 1. 55-56 cm; 2. 41-42 cm; 3. 95-96 cm; 4. 41-42 cm; 5. 90-91 cm; 6. 94-95 cm; 7. 91-92 cm; 8. 91-92 cm; 9. 45-46 cm; 10. 100-101 cm; 11. 81-82 cm. Plates12-17 Regular-sized *Micula* spp. 12. 44-45 cm; 13. 41-42 cm; 14. 51-52 cm; 15. 105-106 cm; 16. 97-98 cm; 17. 36-37 cm. Plates 19-20 Regular-sized *Retecapsa* spp. 19. 85-86 cm; 20. 100-101 cm. 18, 21, 22 Small *Retecapsa* spp. 21. 71-72 cm, 22. 100-101 cm, 18. 100-101 cm. Scale bar, 2 μm.

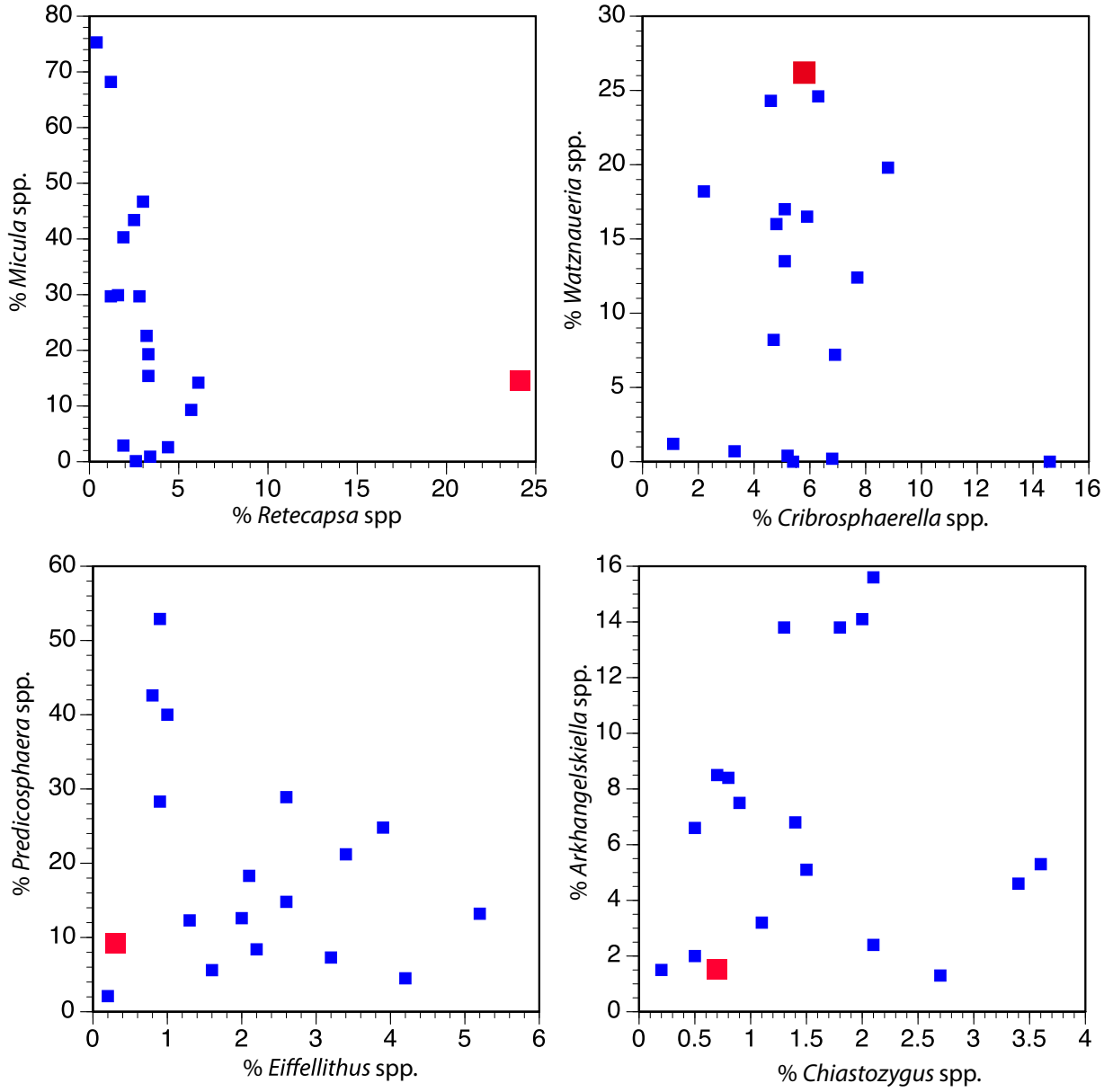

Extended Data Figure 6. Relative abundance of major Maastrichtian calcareous nannoplankton. Small blue squares are Maastrichtian sites from the global compilation[12]; larger red squares are from the transitional unit at Site M0077. These data demonstrate the unusual abundance of *Watznaueria* and *Retecapsa* at Site M0077.

Supplementary Materials:

Helium Isotope Age Model

Age Interpretations

References (*39-41*)

Table S1-S3

Constructing the ^{3}He-based Age Model

The total extraterrestrial ^{3}He ($^3He_{ET}$) concentration in the transitional unit will be the sum of $^3He_{ET}$ delivered from space during its deposition in the Danian plus any $^3He_{ET}$ that comes from reworked Maastrichtian (or earlier) sediment.

Dropping the ET subscript for simplicity and using subscripts tot for total, D for Danian, and RM for reworked Maastrichtian:

$$^3He_{tot}=^3He_D +^3He_{RM}$$

The Danian ^{3}He component is given by the extraterrestrial ^{3}He flux (f_3, taken from Mukhopadhyay et al.[39] divided by the total mass accumulation rate (α_{tot}) of the transitional unit. Here the term total is used to indicate that there are both reworked Maastrichtian and "new" Danian sediments contributing to the sediment flux:

$$^3He_D=f_3/\alpha_{tot}$$

The concentration of reworked Maastrichtian ^{3}He in the transitional unit depends on the concentration of ^{3}He in reworked Maastrichtian sediment (^3He_M) and the mass fraction of reworked Maastrichtian sediment (F_{RM}) in the transitional unit.

$$^3He_{RM}=F_M\ ^3He_M$$

The ^{3}He concentration of Maastrichtian sediment is governed by the extraterrestrial ^{3}He flux and the Maastrichtian mass accumulation rate (α_M). Assuming that f_3 did not change between Maastrichtian and Danian (i.e., f_3 is constant), and further assuming no separation of extraterrestrial particles from bulk sediment during reworking:

$$^3He_M= f_3/\alpha_M$$

Combining these equations:

$$^3He_{tot}= f_3/\alpha_{tot} + F_M f_3/\alpha_M = f_3\ (1/\alpha_{tot} + F_M/\alpha_M) \qquad \text{[eq. 1]}$$

There are two obvious endmember scenarios of interest for understanding the transitional unit. The first assumes no reworking of Maastrichtian sediment carrying pre-impact extraterrestrial ^{3}He. In this scenario, F_M=0. Rearranging equation 1 to solve for mass accumulation rate yields:

$$\alpha_{tot} = f_3/^3He_{tot} \qquad \text{[eq. 2]}$$

In this scenario α_{tot} is a firm lower limit on the sediment mass accumulation rate.

A second endmember scenario of interest assumes that the transitional unit was deposited so quickly that syndepositional (i.e., Danian) extraterrestrial ^{3}He accumulation is negligible. In this case the first term in equation 1 is negligible. In this scenario, we can solve for a firm upper limit to the mass fraction of Maastrichtian sediment in the transitional unit.

$$F_M = \alpha_M \, {}^3He_{tot}/f_3 \qquad \text{[eq. 3]}$$

We measured 8 samples of the transitional unit for ^{3}He (Extended Data Table 1). Although there is some variability among these measurements, there is no obvious trend with depth. We therefore use the mean value of these samples in our computations:

$$^3He_{tot} = 0.005 \pm 0.002 \text{ pcc/g } (1\sigma \text{ standard deviation})$$

Estimated sediment mass accumulation rates in the Maastrichtian are poorly known, but we assume a typical value of $\alpha_M \sim 0.44$ g/cm2/kyr, recognizing this is an approximate calculation.

We assume the extraterrestrial ^{3}He flux is the same as determined by (*37*):

$$f_3 = 0.106 \text{ pcc/cm}^2\text{/kyr}$$

Using equation 3 to solve for an upper limit on the fraction of Maastrichtian sediment in the transitional unit yields the remarkably low value of $F_M = 2\%$. Even assuming an order of magnitude faster mass accumulation rate (~5 g/cm^2/kyr) still yields a value of just ~20%. Thus the ^{3}He data indicate that the transitional unit must be dominated by post-impact sediment rather than reworked material (unless extraterrestrial ^{3}He has been very effectively removed from the pre-impact sediment prior to redeposition).

Now considering the second endmember scenario, no reworked Maastrichtian sediment at all in the transitional unit, equation 2 yields a lower limit to the mean mass accumulation rate of the transitional unit of $\alpha_M = 21$ g/cm^2/kyr. Using the measured dry bulk density of the transitional unit of 2.53 g/cm^3, this corresponds to a linear sedimentation rate of ~10 cm/kyr.

Using this lower limit to the linear sedimentation rate, the 76 cm of the transitional unit must have been deposited in < 8 kyr. Note that even a tiny fraction of reworked Maastrichtian sediment would drastically reduce this value (i.e., at 2% reworked Maastrichtian sediment, the transitional unit would be inferred to have accumulated on a timescale too short for detection with the ^{3}He method, < ~ kyr).

Extended Data Table 1 also provides an age model based on this endmember scenario, with the bottom-most sample defined as t=0. In the absence of densely spaced and replicated ^{3}He data, for this calculation we use the mean extraterrestrial ^{3}He concentration of the entire 76 cm of the transitional interval, i.e., the mean sedimentation rate of 10 cm/kyr as computed above. This age model should be understood as providing an upper limit on the age at a given depth given the probability of reworked pre-impact ^{3}He in the transitional unit.

Age interpretations

This paper hinges on robust age interpretations for two key events which are clearly expressed the paleontological record: the first appearance of life in the crater in the upper part of the transitional unit and the establishment of a healthy, productive ecosystem at the base of the Danian limestone.

The most important of these two events is the establishment of a productive ecosystem in the early Danian. Fortunately, this is also the event for which we have the highest confidence age control for the establishment of a productive ecosystem in the early Danian. The lowermost sample in this limestone contains nannoplankton bloom taxa, geochemical markers for high productivity, and a multilayer benthic community that includes diverse and abundant benthic foraminifera and a diverse set of macrobenthic trace fossils. It also contains the lowest occurrence of the key planktic foraminifer *Parvularugoglobigerina eugubina*. This datum defines the base of Planktic Foraminifer Zone Pα, which occurs 30 kyr after the K-Pg boundary, according to the paleomagnetic timescale calibration of Cande and Kent[39] (see also[18,29]). An alternate calibration[40] gives an age 40 kyr after the impact. A difference of 10 kyr between these two calibrations is negligible, and does not change our key result, that the recovery of primary production in the Chicxulub Crater was significantly faster than nearby Gulf of Mexico and North Atlantic sites, which took 300 kyr or longer to achieve similar recovery[10]. A potentially greater source of error is whether or not the base of the limestone is the true base of Zone Pα or whether a condensed interval or period of non-deposition occurs between the lowest occurrence of *P. eugubina* and the top of the transitional unit. We are confident that very little time could be missing from Zone Pα for several reasons. The lowermost few samples are dominated by primitive early Danian forms, primarily *P. eugubina, P. extensa, P. alabamensis*, and *Guembelitria cretacea*[41]. Other taxa that originate in Zone Pα are either very rare or absent in

this lowermost sample, including the genera *Praemurica, Eoglobigerina*, and *Chiloguembelina*. The absence of these more advanced forms suggests that this lowermost sample is early in the zone. We are therefore confident that the establishment of a productive, healthy ecosystem occurred in the Chicxulub Crater within approximately 30 kyr of the impact.

The appearance of life in the Chicxulub Crater within years of the impact is also a highly significant result. Fortunately, we have a number of ways to constrain this occurrence (Figure 3). Based on the biostratigraphy discussed above, we know that the burrows and survivor microfossil species in the upper portion of the transitional unit appeared no later than 30 kyr after the impact. The minimum amount of time, based on the physical and geochemical properties of the rock and assumptions about crater processes, is even shorter, on the order of years. To better constrain this, we utilize the abundance of ^{3}He in the transitional unit. As described above, ^{3}He provides a maximum duration of 8 kyr, assuming none of the ^{3}He is reworked. If we assume that even a small amount of ^{3}He is reworked (very likely, given the prevalence of reworked microfossils), then the transitional unit was deposited in a period of time below the resolution of the ^{3}He proxy, < ~1 kyr.

The most likely mechanism to explain such rapid deposition of fine grained material is settling from suspension from water made turbid by immediate post-impact wave energy. The lower portion of the transitional unit is interspersed with higher energy deposits which record the waning energy of tsunami, seiche and other water mass movements generated by the impact resurge, and platform margin collapses. Our interpretation of sedimentary settling from turbid water is bolstered by the homogeneous sedimentary makeup of the unit, as well as Site M0077's position on the bathymetric high of the peak ring. To further refine the amount of time represented by this unit we can apply Stokes' law (assuming a water depth of 650 m, a minimum

particle size of 2 μm, and applying the density of carbonate – 2.7 g/cm^3), which indicates the smallest particles in this unit took approximately 6 years to completely settle out of suspension. This is likely over estimates the true settling time, as most of the grains are larger than 2 μm and the presence of multiple laminae in the lower portion of the unit indicate that settling wasn't the only process by which this unit was deposited. Despite these caveats, Stokes' Law provides a useful constraint on the time scales involved, and allows us to state with confidence that life first appeared in the crater within years after the impact.

Supplemental References

39. Cande, S. C. & Kent, D. V. Revised calibration of the geomagnetic polarity timescale for the Late Cretaceous and Cenozoic, *Journal of Geophysical Research* **100**, 6093-6095 (1995).

40. Luterbacher, H. P. et al. The Paleogene Period. In: Gradstein, F., Ogg, J. & Smith, A. (Eds.), *A Geologic Time Scale 2004*. Cambridge University Press, 384-408 (2004).

41. Koutsoukos, E. A. M. Phenotypic plasticity, speciation, and phylogeny in early Danian planktic foraminifera, *Journal of Foraminiferal Research* **44**, 109-142 (2014).

Extended Data Table 1. ^{3}He data.

Sample	start cm	stop cm	^{3}He pcc/g	^{4}He ncc/g	Absolute ^{3}He/^{4}He	Fraction ^{3}He ET	Maximum ^{3}He -Based Model Age (kyr)
KT39	39	40	0.0068	13.6	5.04E-07	0.96	6.0
KT48	48	49	0.0055	35.4	1.56E-07	0.87	4.9
KT59	59	60	0.0064	23.1	2.78E-07	0.92	4.0

KT68	68	69	0.0042	31.6	1.33E-07	0.84	2.9
KT79	79	80	0.0036	18.3	1.99E-07	0.9	1.9
KT89	89	90	0.0105	34.7	3.04E-07	0.93	0.9
KT99	99	100	0.0045	64.3	6.99E-08	0.70	0.1
KT106.5	107	108	0.0109	327	3.32E-08	0.37	0.0

Supplementary Information is linked to the online version of the paper at www.nature.com/nature.

Acknowledgments This research used samples and data provided by IODP. Expedition 364 was jointly funded by the European Consortium for Ocean Research Drilling (ECORD) and ICDP, with contributions and logistical support from the Yucatán State Government and Universidad Nacional Autónoma de México (UNAM). We thank Tessa Cayton for assistance crushing and washing samples; Serena Dameron, Renata Moura de Mello, and Mark Leckie for helpful discussions on benthic foraminifer taxonomy; James Maner for assistance with the UT ESEM laboratory and Rowan Martindale for assistance with petrographic microscope imaging. We are particularly grateful for assistance of the staff of the IODP Core Repository in Bremen, Germany for their assistance taking these samples and running "shipboard" analyses. The authors acknowledge Post-Expedition Awards from the U.S. Science Support Program for CL and TB, NSF OCE 1737351, and NASA NNX16AJ60G. Funding for FR-T was provided by Project CGL2015-66835-P (Secretaría de Estado de I+D+I, Spain), and Scientific Excellence Unit UCE-2016-05 (Universidad de Granada).

Author Contributions All authors participated in sampling and data collection offshore and/or onshore during IODP/ICDP Expedition 364. CML, TJB, FJR, HJ, and JS collected and analyzed microfossil data, MTW provided detailed sedimentology, JDO, PC, and KF collected trace element, XRF, and He isotope data, respectively. All authors contributed to writing/editing of the manuscript.

Author Information Reprints and permissions information is available at www.nature.com/reprints. The authors declare no competing financial interests. Readers are welcome to comment on the online version of the paper. Correspondence and requests for materials should be addressed to CML (cmlowery@utexas.edu).

Reviewer Information [to come]